Angle of optical rotation measurement with differential polarimetry

Markus Schake
Physikalisch-Technische Bundesanstalt, Bundesallee 100, 38116 Braunschweig, Germany
mailto:markus.schake@ptb.de

1 Introduction and measurement setup

The Physikalisch-Techniche Bundesanstalt (PTB) in Braunschweig, offers a calibration service for the angle of optical rotation (OR) of Quartz glass plates. Such Quartz plates are used as calibration standards in the sugar industry. The optical rotation of light passing a solution of water and sugar shows a characteristic dependency of the sugar concentration. The optical rotation of quartz [1] is linked to the optical rotation of sugar solutions by the international sugar scale [2, 3].

Among commonly used modern polarimeters for differential OR measurements there are two general measurement principles:

- Model (A): Superposition of the static OR of the SUT with a periodical modulation introduced by a Faraday modulator to implement lock-in detection of the polarizer extinction [4].
- Model (B): Continuously rotating linear polarizer to modulate the detected intensity and to determine the static OR of the SUT from the signal phase [5].

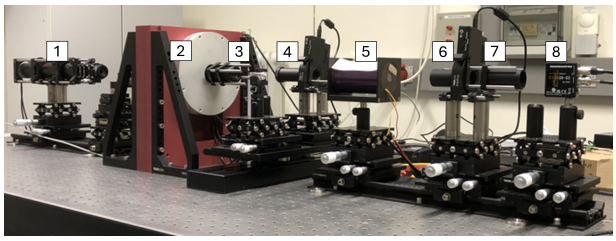

Fig. 1 *Photograph of the new polarimeter at PTB: (1) Light source, (2) rotation stage, (3) linear polarizer, (4) sample under test (SUT), (5) Faraday modulator, (6) rotation stage, (7) linear polarizer, (8) photodiode.*

The setup used at PTB is a model (A) differential polarimeter. The device currently used for the calibration service for the angle of optical rotation is operated since the early 1950s and has been modernized multiple times. However, replacement parts for the old device are no longer available, and it will soon be replaced with a new polarimeter. The new device is also a model (A) polarimeter and is depicted in Fig. 1. The linear polarizers (3) and (7) form a cavity containing the SUT (4) and the Faraday modulator (5). During motion of the accurate rotation stage (2), the photodiode is detecting an intensity signal of the form:

$$I_{PD}(x,y,t) = \frac{1}{2} I_0 \cdot [\, 1 + \cos\left(2(\Delta\phi_p(x,y) + \alpha_s(x,y) + \beta_F(x,y) \cdot \sin(2\pi f_F \cdot t))\right)] \tag{1}$$

$I_{PD} \rightarrow$ intensity observed at the photo diode
$I_0 \rightarrow$ amplitude of intensity
$\Delta\phi_p(x,y) \rightarrow$ angle difference of (3) and (7)
$\alpha_s(x,y) \rightarrow$ OR of the SUT
$\beta_F(x,y) \rightarrow$ OR amplitude of the Faraday modulator
$f_F \rightarrow$ frequency of the Faraday modulator
$t \rightarrow$ time
$(x,y) \rightarrow$ lateral coordinate

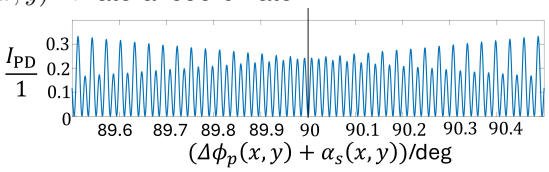

Fig. 2 *Photodiode signal close to the extinction point.*

In proximity of the extinction points, where $\Delta\phi_p(x,y) + \alpha_s(x,y) = n \cdot \frac{\pi}{2} \forall n = 1,3,5,\ldots$ a characteristic signal form as depicted in Fig. 2 is detected, in which the signal component at the modulation frequency f_F vanishes. At the same time the signal component with the frequency $2f_F$ reaches its maximum. The signal modulation enables the application of different algorithms for extinction point detection, not only by signal amplitude but also by signal phase and other frequency domain metrics. Detection of the extinction point causes a trigger signal to stop the rotation stage (2) and its angular position is recorded.

2 Measurement procedure and data evaluation

A typical measurement cycle to obtain the OR of a SUT contains:

- Detection of extinction point with empty cavity
- Detection of extinction point with SUT

The sample OR is directly calculated from the angular position difference of the rotation stage (2)

DGaO Proceedings 2025 – *http://www.dgao-proceedings.de* – ISSN: 1614-8436 – urn:nbn:de:0287-2025-P022
submitted: 03.07.2025 – published: 30.09.2025

when stopped by the trigger in the respective extinction positions. Therefore the trigger position error ΔOR directly increases the OR uncertainty. To find noise robust implementations, multiple algorithms have been compared. The currently employed algorithm for OR measurement is based on a sliding Lock-In detection as described in Fig. 3.

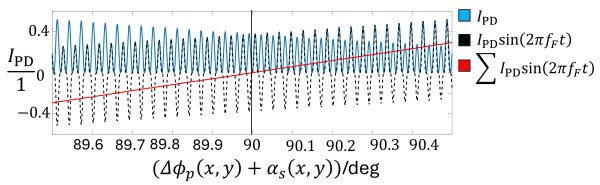

Fig. 3 *Sliding Lock-In detection: The sampled section of the signal $I_{PD}(t)$ is multiplied with $\sin(2\pi f_F \cdot t) \forall t \in [\tau_1, \tau_2]$ to implement a frequency Lock-In. The zero crossing of $\sum I_{PD}(t) \cdot \sin(2\pi f_F \cdot t)$ is detected and causes a trigger.*

For comparison an algorithm for zero crossing detection based on a sliding Fourier transform filter (Fig. 4) and a sliding phase evaluation filter (Fig. 5) are employed.

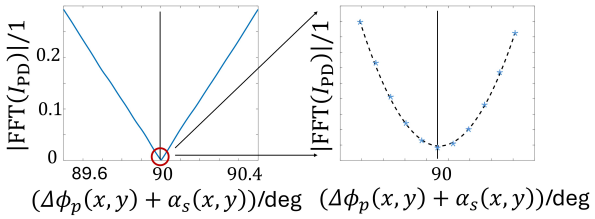

Fig. 4 *Sliding FFT and fitting: The sampled section of the signal $I_{PD}(t)$ is Fourier transformed and its power spectral density $|FFT(I_{PD}(t))|$ is monitored for its minimum at the frequency f_F.*

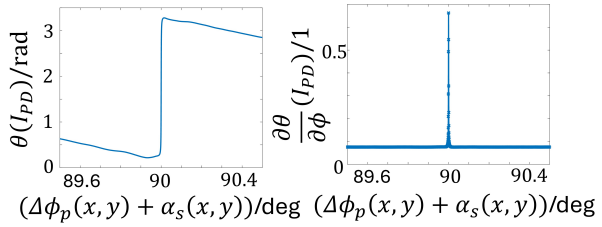

Fig. 5 *Sliding phase evaluation: The sampled section of the signal $I_{PD}(t)$ is Fourier transformed and the real and imaginary parts of its Fourier Transform at the frequency f_F are used to calculate the signal phase $\theta(I_{PD})$. a) Nonlinear part of the unwrapped signal phase. b) Gradient of the phase $\theta(I_{PD})$ with respect to the rotation angle ϕ.*

All filters have in common, that they might be implemented in real time systems and cause a trigger pulse when the extinction point is passed by the rotation stage (2). To evaluate the performance of these algorithms with respect to their robustness against noise in the sampled signal, they are implemented in a simulation environment. The photodiode signal as described in Eq. (1) is mixed with white noise with an amplitude, which is equal to 5% of the intensity modulation caused by the Faraday modulator amplitude β_F.

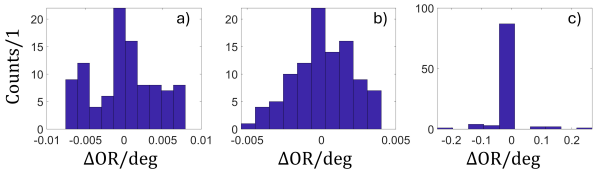

Fig. 6 *OR error ΔOR distribution for white noise (5% of β_F) with $N = 100$ samples: a) Sliding Lock-In detection, b) Sliding FFT and fitting, c) sliding phase evaluation.*

A series of $N = 100$ virtual experiments is performed in which the different methods are applied to identify the extinction point of the polarizers. The white noise is generated for each experiment individually. Fig. 6 shows the error distributions ΔOR of the detected extinction points. The standard deviation σ observed for the Lock-In detection (Fig 6 a)) is $\sigma = 0.0041$ deg, for the sliding FFT filter (Fig 6 b)) $\sigma = 0.0020$ deg and for the sliding phase filter (Fig 6 c)) $\sigma = 0.050$ deg. This indicates, that the implementation of the sliding Fourier transform filter into the experimental setup might yield an improvement in terms of noise robustness. However, the implementation of the Fourier transform on the real time Microcontroller system might cause an increase of runtime due to its more complex calculations. The noise levels observed in the real system are much smaller, than those observed in the simulation making the overall improvement in the performance of the setup less significant than they would appear from the simulation results. The expanded measurement uncertainty of the OR measurement at PTB is specified as $U = 0.0010$ deg for coverage factor $k = 2$ and assuming a normal distribution. The influence of signal noise on the measured OR may be estimated to be approximately $u_{\text{noise}} \approx 0.0002$ deg as observed in repeated measurements under constant environmental conditions.

In conclusion, further improvements with respect to noise robustness may contribute to a reduction of the expanded measurement uncertainty.

References

[1] T. Matsuura and H. Koshima, “Introduction to chiral crystallization of achiral organic compounds: Spontaneous generation of chirality,” Journal of Photochemistry and Photobiology C: Photochemistry Reviews **6**(1), 7–24 (2005). URL `https://www.sciencedirect.com/science/article/pii/S1389556705000055`.

[2] *ICUMSA 22nd Session* (Berlin: ICUMSA, 1998).

[3] *OIML R 14 Polarimetric saccharimeters graduated in accordance with the ICUMSA International Sugar Scale* (OIML, 1995).

[4] E. Castiglioni, S. Abbate, and G. Longhi, “Experimental methods for measuring optical rotatory dispersion: Survey and outlook,” Chirality **23**(9), 711–716 (2011). `https://doi.org/10.1002/chir.20981`.

[5] A. J. Harvie, T. W. Phillips, and J. C. deMello, “A high-resolution polarimeter formed from inexpensive optical parts.” Sci Rep **10**, 5448 (2020). `https://doi.org/10.1038/s41598-020-61715-7`.